THE JOURNAL OF PHYSICAL CHEMISTRY C

Article

pubs.acs.org/JPCC

NMR Relaxometric Properties of SPION-Loaded Solid Lipid Nanoparticles

Lucia Calucci,[*,#] Agostina Grillone,[§,†] Eugenio Redolfi Riva,[§] Virgilio Mattoli,[§] Gianni Ciofani,[§,‡] and Claudia Forte[#]

[#]Istituto di Chimica dei Composti OrganoMetallici, Sede Secondaria di Pisa, Consiglio Nazionale delle Ricerche − CNR, Via G. Moruzzi 1, 56124 Pisa, Italy

[§]Istituto Italiano di Tecnologia, Center for Micro-BioRobotics @SSSA, Viale Rinaldo Piaggio 34, 56025 Pontedera (Pisa), Italy

[†]Scuola Superiore Sant'Anna, The BioRobotics Institute, Viale Rinaldo Piaggio 34, 56025 Pontedera (Pisa), Italy

[‡]Politecnico di Torino, Department of Mechanical and Aerospace Engineering, Corso Duca degli Abruzzi 24, 10129 Torino, Italy

ABSTRACT: Longitudinal and transverse relaxivities of solid lipid nanoparticles loaded with superparamagnetic iron oxide nanoparticles (SPION-SLNs) were thoroughly investigated with the aim of understanding the main parameters regulating the potential negative contrast properties of these systems. In particular, the longitudinal relaxivity (r_1) of water protons in the 10 kHz to 35 MHz frequency range was determined by ^{1}H fast field-cycling NMR, while transverse relaxivity (r_2) was measured at 21 MHz. The reproducibility and stability of SPION-SLNs was also tested on samples arising from independent preparations and at different times after preparation. Water diffusion in proximity of superparamagnetic nanoparticles was found to be the mechanism of proton nuclear relaxation enhancement and characteristic parameters were quantitatively determined by fitting the experimental data acquired on different samples as a function of concentration and temperature. Although a variation ascribable to the formation of clusters with a different number of SPIONs inhomogeneously embedded in the lipid matrix was observed among different preparations, the relaxivity properties of the investigated SPION-SLNs were found to be better than those of SPION-based contrast agents commonly considered as standard in the literature, and remained stable for at least 2 months.

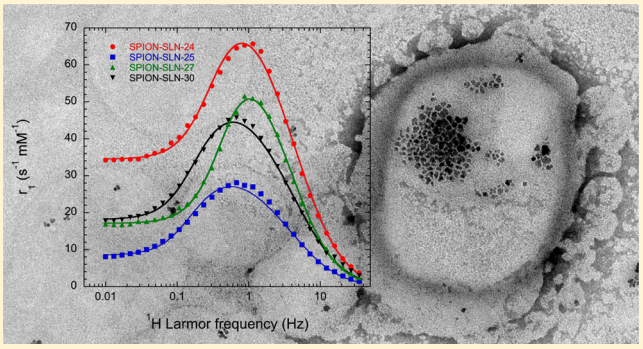

INTRODUCTION

Superparamagnetic iron oxide nanoparticles (SPIONs) are nanosystems with good biocompatibility,[1−3] currently attracting much scientific interest because of their potential uses in biomedicine for both diagnosis and therapy.[4−13] Indeed, SPION applications such as drug and gene-targeted delivery,[14,15] hyperthermia,[16,17] biosensing,[18] and contrast enhancement for magnetic resonance imaging (MRI),[19−23] have been extensively investigated. The biological and magnetic properties and the related potential applications of SPIONs in these fields are affected by their shape and size, as well as by the coating materials used to stabilize these particles in aqueous media.[24−30] In particular, r_2 relaxivity (i.e., the water proton transverse relaxation rate given per millimole of iron per liter of solution), which is a property determinant for the applicability of magnetic nanoparticles as MRI negative contrast agents, has been found to be enhanced when SPIONs are embedded into an organic matrix, where they form clusters.[11,22,31−35] In the clusters, SPIONs retain their superparamagnetic properties, and each cluster can be considered as a large magnetized particle with a magnetic moment proportional to its size. As a consequence, r_2 depends on cluster magnetization and, analogously to single-core nanoparticles, SPION clusters show three different r_2 regimes depending on their size: motional average regime (MAR), static dephasing regime (SDR), and echo-limiting regime (ELR). In addition, the self-assembly structure and the nanoparticle arrangement in the organic matrix significantly affect transverse relaxivity.[11,22,31,36] Finally, the resulting nanoassemblies are subject to stability issues and size limitations for *in vivo* applications.[37]

In a recent work,[38] we showed that nanovectors with promising properties for application in theranostics can be prepared by loading solid lipid nanoparticles (SLNs) made of cetyl palmitate with the anticancer drug sorafenib and SPIONs (average diameter of 10 nm) by a hot homogenization technique. SLNs guarantee a high drug loading efficiency (about 90%) and a high stability in water. SPION-loaded SLNs (SPION-SLNs) exhibit good cytocompatibility, whereas an antiproliferative effect against tumor cells (human hepatocarcinoma HepG2) is imparted to the nanoparticles by sorafenib.

Received: September 21, 2016
Revised: December 1, 2016
Published: December 2, 2016

DOI: 10.1021/acs.jpcc.6b09562
J. Phys. Chem. C 2017, 121, 823−829

SPIONs were found to maintain their superparamagnetic properties and saturation magnetization when embedded in the SLN matrix, thus enabling the movement/targeting of SLNs in the presence of a remote magnetic field and conferring to SLNs negative contrast properties for MRI. In particular, r_2 was found to be 38 ± 2 s^{-1} mM^{-1} at 7.05 T and 215 ± 5 s^{-1} mM^{-1} at 0.47 T, and the ratio between transverse and longitudinal relaxivities, r_2/r_1, was 633 at 7.05 T and 77 at 0.47 T, values higher than those of the most common SPION-based contrast agents at magnetic fields of clinical interest.[19,39−44]

Here, the NMR relaxometric properties of SPION-SLNs are investigated in detail by measuring the longitudinal ($R_1 = 1/T_1$) relaxation rate, and consequently the longitudinal relaxivity (r_1), of water protons at different Larmor frequencies and analyzing them in terms of theoretical models for relaxation induced by superparamagnetic particles.[45−48] To this aim, ^{1}H R_1 data were acquired on SPION-SLN suspensions at different concentrations and temperatures over the 0.01 to 35 MHz frequency range using a fast field-cycling (FFC) relaxometer. Therefore, an analysis of the nuclear magnetic resonance dispersion (NMRD) profiles of r_1 was performed to obtain qualitative and quantitative information on the relaxation mechanism dominating water proton relaxation in these systems. In addition, the reproducibility and stability of SPION-SLNs, two properties of relevance for medical applications,[49−51] were tested by measuring r_1 and r_2 values on samples arising from independent preparations and at different times.

EXPERIMENTAL SECTION

Materials. The SPION-loaded SLN samples were prepared by using an oil-in-water homogenization process at high temperature, as reported in ref 38. In detail, 210 mg of cetyl palmitate (kindly provided by Gattefossé) and 15 mg of SPIONs (EMG1300 from Ferrotec; average nominal diameter 10 nm; saturation magnetization at 300 K 60 emu/g[38]) were dissolved in 1 mL of chloroform. The methanol and chloroform solutions were added and gently stirred. The obtained mixture was then transferred into a vial containing 3 mL of a Tween 80 (Sigma-Aldrich) water solution (6%) and sonicated for 5 min with a probe-tip ultrasonicator (SONOPLUS mini20, Bandelin). To allow organic solvents evaporation, the temperature of the emulsion was kept constant at 75 °C using a homemade heater system with a negative feedback control. The obtained dispersion was kept at 4 °C for 15 min to allow the formation of the SLNs. The final product was purified by gel chromatography, using Sephadex G-25 prepacked columns (GE Healthcare Life Sciences) and deionized water as eluent.

Four independent preparations were performed, in the following indicated as SPION-SLN-24, SPION-SLN-25, SPION-SLN-27, and SPION-SLN-30, with the number indicating the SPION-SLN concentration in mg/mL. For r_1 and r_2 determinations, SPION-SLN suspensions at different concentrations were prepared by dilution with ultrapure water.

The Fe content was determined by inductively coupled plasma-mass spectrometry (ICP-MS, Agilent Technologies Inc., 7700 series) on samples treated with 65% HNO_3 and 30% H_2O_2 and digested in a Milestone Start D microwave apparatus.

Determination of Relaxivity Values. Longitudinal relaxation times of water protons were acquired over the Larmor frequency range 0.01−35 MHz with a Spinmaster FFC-2000 fast field-cycling NMR relaxometer (Stelar srl, Mede, Italy). T_1 measurements were performed using the prepolarized (PP) and nonpolarized (NP) pulse sequences[52,53] below and above 12 MHz, respectively. The polarizing (B_{pol}) and detection (B_{acq}) fields were 0.70 and 0.50 T, corresponding to ^{1}H Larmor frequencies of 30.0 and 21.5 MHz, respectively. The switching time was 3 ms, the 90° pulse duration was 10 μs, and a single scan was acquired. All the other experimental parameters were optimized for each measurement. All the ^{1}H magnetization curves versus time were monoexponential within experimental error, and the errors in T_1 fitting were always less than 1%. The temperature was controlled within ±0.1 °C with a Stelar VTC90 variable temperature controller.

T_2 measurements of water protons were performed at 21 MHz using a Niumag permanent magnet interfaced with a Stelar PCNMR console. The CPMG pulse sequence was applied with an echo delay of 30 μs and a 90° pulse duration of 3 μs. The temperature was controlled within ±0.1 °C with a Stelar VTC90 variable temperature controller.

Relaxation rates (R_i) were calculated as the inverse of the relaxation times ($R_i = 1/T_i$) and relaxivity values (r_i) were determined on the basis of the iron concentration [Fe] of the samples by fitting data acquired on SPION-SLNs aqueous suspensions at different concentrations to the equation:

$$R_i = R_{i,0} + r_i[\mathrm{Fe}] \quad (1)$$

where $R_{i,0}$ is the relaxation rate in pure water.

Analysis of NMRD Curves. NMRD curves were analyzed using a purposely written nonlinear least-squares fitting program within the Mathematica environment on the basis of eq 1 and eqs 2−7 reported in the Results and Discussion section.

RESULTS AND DISCUSSION

^{1}H R_1 NMRD curves (Larmor frequency between 0.01 to 35 MHz) were acquired at 37 °C on aqueous suspensions of four SPION-SLN samples (SPION-SLN-24, SPION-SLN-25, SPION-SLN-27, and SPION-SLN-30) independently prepared following the same procedure (see the Experimental section). In all cases, the R_1 profiles showed a low frequency plateau, a prominent peak, referred to as the Curie peak, with maximum between 0.7 and 1.1 MHz, and a rapidly decreasing trend at high frequencies (Figure 1). These profiles are characteristic of

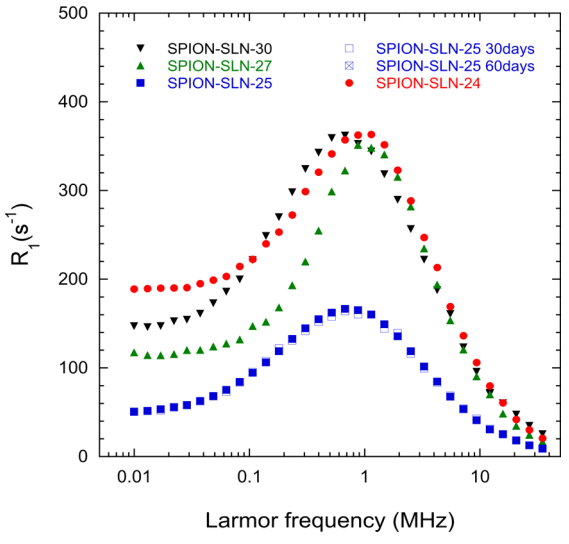

Figure 1. ^{1}H longitudinal relaxation rates of different SPION-SLN samples at 37 °C.

DOI: 10.1021/acs.jpcc.6b09562
J. Phys. Chem. C 2017, 121, 823−829

water proton relaxation induced by superparamagnetic nanoparticles,[4,19,20,45] in agreement with the magnetic properties of these systems previously reported on the basis of magnetometric measurements.[38] In these cases, the mechanism driving nuclear relaxation at low frequencies depends directly on the magnetic anisotropy of the magnetic particles, while at high frequencies, Curie relaxation, which arises from the diffusion of water molecules in the presence of the magnetic moments, becomes dominant.

NMRD curve shapes differing in the low frequency plateau value, in the frequency of the Curie peak maximum, and in the maximum R_1 value were observed for the different samples, suggesting dissimilarity in the SPION distribution inside the SLNs. Indeed, as reported by us in a previous paper,[38] while dynamic light scattering (DLS) measurements gave an average diameter value of 248 ± 113 nm with a satisfactory polidispersity index (0.2 ± 0.1), both AFM and TEM investigations gave strong indications of the presence of SPIONs both internalized and on the surface of SLNs.

On the contrary, perfectly reproducible NMRD curves were obtained by repeating the R_1 measurements at different times on the same sample; as an example, NMRD curves acquired after 1 and 2 months on the SPION-SLN-25 sample are shown in Figure 1. Considering the high sensitivity of NMRD profiles to the size of dispersions and to nanoparticle aggregation, this behavior represents a strong indication of a very good long-term stability of SPION-SLN suspensions, in agreement with previous *Z*-potential measurements (−23.0 ± 5.3 mV) that indicated a good colloidal stability of SPION-SLNs in an aqueous environment.[38]

In order to better compare the different SPION-SLN preparations, r_1 values were determined by acquiring R_1 NMRD profiles on suspensions at different concentrations obtained by dilution of each original sample. A linear dependence of R_1 on concentration was found at each frequency for all SPION-SLN samples, indicating that there are no concentration-dependent aggregation effects of SLNs and that suspensions are stable to dilution with water. A linear fit (eq 1) was therefore applied to determine r_1 values at all frequencies taking Fe concentration values measured by ICP-MS, which were 5.51, 6.20, 6.88, and 8.06 mM for SPION-SLN-24, SPION-SLN-25, SPION-SLN-27, and SPION-SLN-30, respectively. The profiles of r_1 vs Larmor frequency, shown in Figure 2, indicate that the variation in relaxivity of SPION-SLNs samples arising from different preparations cannot be accounted for by differences in Fe and, therefore, SPION concentration. It must be pointed out that the measured Fe concentration values are proportional to SPION-SLN concentration values in the examined suspensions, indicating that SPION loading is on average equal for all preparations. Therefore, the different relaxivity properties must be related to a variety of SPION distributions inside the cetyl palmitate matrix. However, since the curves retain the characteristics of superparamagnetic relaxation, it seems that agglomeration, which would cause flattening out of the maximum, is not relevant.[54]

In order to single out the parameters regulating the observed behavior, r_1 vs ^{1}H Larmor frequency profiles were analyzed in terms of the euristic model proposed by Roch et al.[4,45,46] for describing the relaxation enhancement of protons in water molecules diffusing in proximity of superparamagnetic particles. Following this model, in the high anisotropy approximation, justified by the absence of dispersion at low frequency in the

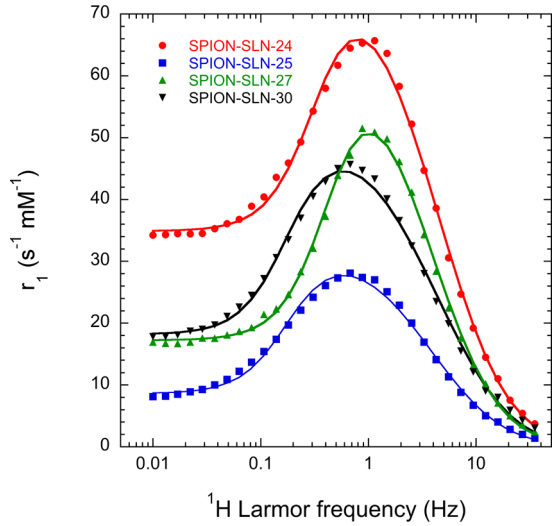

Figure 2. Experimental (symbols) and calculated (lines) ^{1}H longitudinal relaxivity values of different SPION-SLN samples at 37 °C.

NMRD curves, the dependence of the longitudinal relaxation rate R_1 on the proton angular Larmor frequency ω can be written as

$$R_1(\omega) = C\tau_d\left\{\left[7\frac{L(x)}{x} + 3\left(1 - 2\frac{L(x)}{x} - L^2(x)\right)\right] \times J_F(\omega, \tau_d, \tau_N) + 3L^2(x)J_A(\omega, \tau_d)\right\} \quad (2)$$

where τ_N is the Néel relaxation time, and τ_d is the translational diffusion correlation time; τ_d is connected to d, the distance of closest approach of the water molecules to the SPION clusters giving rise to water proton relaxation enhancement, by the relationship $\tau_d = d^2/D$, D being the relative translational diffusion coefficient (i.e., the sum of the diffusion coefficients of the cluster and water). $L(x)$ is the Langevin function given by

$$L(x) = \coth(x) - \frac{1}{x} \quad (3)$$

and

$$x = \frac{\mu B}{k_B T} \quad (4)$$

where B is the magnetic field, μ is the magnetic moment of the SPION clusters, k_B the Boltzmann constant, and T is the temperature. C is a quantity directly proportional to the number of clusters and to μ^2, and inversely proportional to d^3; in cgs units, C can be expressed as

$$C = \frac{32\pi}{135000}\mu^2\gamma_H^2\frac{N_a C_p}{d^3} \quad (5)$$

where γ_H is the gyromagnetic ratio of the proton, N_a is the Avogadro number, and C_p is the molar concentration of clusters.

The spectral densities in eq 2 are expressed by

$$J_A(z) = \frac{1 + 5z/8 + z^2/8}{1 + z + z^2/2 + z^3/6 + 4z^4/81 + z^5/81 + z^6/648} \quad (6)$$

with $z = (2\omega\tau_d)^{1/2}$, and

DOI: 10.1021/acs.jpcc.6b09562
J. Phys. Chem. C 2017, 121, 823−829

Table 1. Best Fitting Values of τ_d, τ_N, and μ Determined by Analyzing r_1 versus Larmor Frequency Profiles at 37 °C Reported in Figure 2 and Calculated Values of d and C_p

sample	τ_d (s)	τ_N (s)	μ (erg/G)	d (nm)[a]	C_p (M)[b]
SPION-SLN-24	$(9.0 \pm 0.1)10^{-8}$	$(1.6 \pm 0.1)10^{-8}$	$(12.8 \pm 0.4)\ 10^{-16}$	16.4	2.1×10^{-8}
SPION-SLN-25	$(9.7 \pm 0.1)10^{-8}$	$(1.7 \pm 0.1)10^{-8}$	$(24.7 \pm 0.6)10^{-16}$	17.1	2.6×10^{-9}
SPION-SLN-27	$(12.3 \pm 0.2)10^{-8}$	$(1.9 \pm 0.1)10^{-8}$	$(9.5 \pm 0.2)10^{-16}$	19.2	5.6×10^{-8}
SPION-SLN-30	$(8.2 \pm 0.1)10^{-8}$	$(1.6 \pm 0.1)10^{-8}$	$(24.7 \pm 0.6)10^{-16}$	15.7	4.7×10^{-9}

[a]Calculated assuming $D = 3 \times 10^{-5}$ cm^2/s. [b]Calculated from eq 5 using best fit values of C and μ, and calculated d values reported in this table.

$$J_F(\Omega) = \mathrm{Re}\left[\frac{1 + \Omega^{1/2}/4}{1 + \Omega^{1/2} + 4\Omega/9 + \Omega^{3/2}/9}\right] \quad (7)$$

with $\Omega = (i\omega + 1/\tau_N)\tau_d$. The r_1 profiles were fitted to obtain optimized values of C, τ_d, τ_N, and μ. As shown in Figure 2, the applied model reproduced experimental data quite well; the best fitting parameter values are reported in Table 1.

The diffusion correlation time, τ_d, was found to be ~82, 90, 97, and 120 ns for samples SPION-SLN-30, SPION-SLN-24, SPION-SLN-25, and SPION-SLN-27, respectively. These differences could be related either to the distance of closest approach (d) of water protons to superparamagnetic particles, that is to SPION clusters embedded in cetyl palmitate, or to the translational diffusion coefficient (D), which could change because of the interactions of water with the lipid matrix. Assuming the same D value for all the samples and coincident with the diffusion coefficient of water at 37 °C ($D = 3 \times 10^{-5}$ cm^2/s),[55] d values 3−4 times larger than the 5 nm radius declared for pristine SPIONs, but sensibly smaller than the hydrodynamic radius of SPION-SLNs,[38] were determined (see Table 1). In particular, a larger d was calculated for sample SPION-SLN-27 (~19 nm) with respect to the other samples, d being less than 16 nm for SPION-SLN-30 and ~17 nm for SPION-SLN-24 and SPION-SLN-25. On the other hand, if changes of τ_d arose from different water diffusion properties in the samples, d values on the order of the pristine SPION radius would be compatible with D values 10 times smaller than that of bulk water. In this case, taking d equal for all the samples, D would increase in the order SPION-SLN-27, SPION-SLN-25, SPION-SLN-24, SPION-SLN-30. However, since the coating material is the same for all samples, differences in D are not expected; thus the most probable origin of the different τ_d values lies in the different internalization of SPIONs, which affects the distance of closest approach.

The validity of the relaxation model used in the analysis of NMRD profiles was confirmed by data acquired at different temperatures in the range between 27 and 47 °C on sample SPION-SLN-30 (Figure 3). By increasing the temperature, a decrease in the relaxation rate, and consequently in the relaxivity, was observed, especially at low frequencies. An analysis of the r_1 profiles on the basis of eqs 1−7 showed that by increasing the temperature there is a slight decrease of τ_d and a more definite decrease of τ_N (see Table 2). The τ_d trend is compatible with the fact that the water diffusion coefficient increases with temperature. On the other hand, the trend of τ_N versus temperature can be well reproduced by an Arrhenius law with an anisotropy energy[4] of 0.93 ± 0.04 GHz.

Thus, considering the validity of the model and the analytical approach used, the best fit parameters obtained for the different samples at 37 °C can be discussed in order to understand the possible phenomena at the basis of the different relaxometric behavior observed. The parameters that show highest variability are μ, the overall magnetic moment of the small clusters of

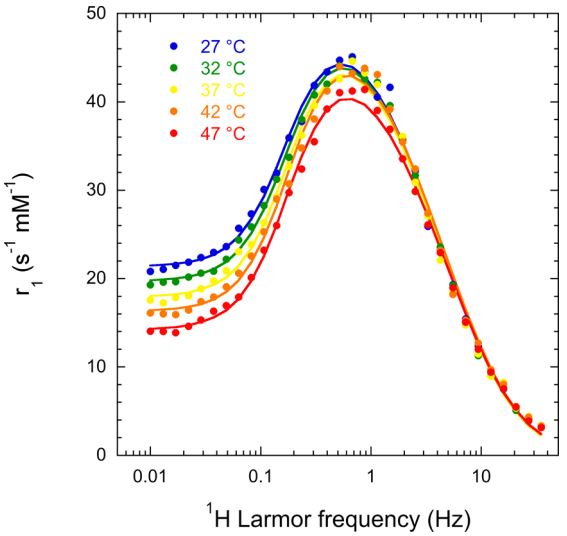

Figure 3. Experimental (symbols) and calculated (lines) ^{1}H longitudinal relaxivity of SPION-SLN-30 at the indicated temperatures.

Table 2. Best Fitting Values of τ_d and τ_N Determined by Analyzing r_1 versus Larmor Frequency Profiles of SPION-SLN-30 at Different Temperatures (Figure 3)

T (°C)	τ_d (s)	τ_N (s)
27	$(8.2 \pm 0.1)10^{-8}$	$(2.1 \pm 0.1)10^{-8}$
32	$(8.2 \pm 0.1)10^{-8}$	$(1.9 \pm 0.1)10^{-8}$
37	$(8.2 \pm 0.1)10^{-8}$	$(1.6 \pm 0.1)10^{-8}$
42	$(7.9 \pm 0.1)10^{-8}$	$(1.3 \pm 0.1)10^{-8}$
47	$(7.7 \pm 0.1)10^{-8}$	$(1.1 \pm 0.1)10^{-8}$

SPIONs inducing water proton relaxation enhancement, and C_p, which is proportional to the number of clusters. By considering the overall magnetic moment as the sum of the magnetic moments of single SPIONs embedded in a cluster,[4,56] we can infer that, on average, larger clusters were formed in samples SPION-SLN-25 and SPION-SLN-30. In general, a higher μ value broadens the Curie peak, and this is indeed observed for SPION-SLN-25 and SPION-SLN-30, which have the highest μ values. The maximum value of r_1 is determined by $\mu^2 C_p/d$[Fe], which decreases in the order SPION-SLN-24, SPION-SLN-27, SPION-SLN-30, SPION-SLN-25. On the basis of these results the different behaviors observed are to be ascribed to a distribution of SPIONs within the cetyl palmitate matrix varying in cluster size and proximity to the SLN/water interface and/or to the rate of water diffusion around the nanoparticles.

An analogous variability was also observed for r_2, measured at 21 MHz and 37 °C, which was found equal to 325 ± 5 s^{-1} mM^{-1}, 230 ± 5 s^{-1} mM^{-1}, and 243 ± 5 s^{-1} mM for SPION-SLN-24, SPION-SLN-25, and SPION-SLN-27, respectively,

DOI: 10.1021/acs.jpcc.6b09562
J. Phys. Chem. C 2017, 121, 823−829

with corresponding r_2/r_1 values of 43, 81, and 49. Given the inhomogeneous distribution of SPIONs in these system, it is not possible to fully rationalize the r_2 values on the basis of theories reported in the literature for transverse relaxation enhancement of water protons in the presence of SPIONs.[56,57] The variations observed among the samples are presumably ascribable to differences in cluster magnetic moment and concentration as well as to the different accessibility to water of SPIONs embedded in the cetyl palmitate matrix.[36] Nonetheless, it is worthy of note that the r_2 and r_2/r_1 values measured for our samples are in all cases higher than those reported for the most common SPION-based contrast agents.[42−44]

CONCLUSIONS

The relaxometric study of cetyl palmitate SLNs loaded with SPIONs, prepared using a hot homogenization technique, allowed a detailed characterization of properties useful for application as MRI contrast agents. The analysis of the NMRD curves of samples arising from distinct preparations highlighted a variability in SPION distribution within the lipid matrix which gave rise to noticeable differences in the salient features of longitudinal relaxivity versus frequency trends. In particular, it was found that a different number of SPIONs is present in clusters with different dimensions and accessibility to water.

Notwithstanding the scarce reproducibility of the preparation, the investigated SPION-loaded SLNs always showed very good potential negative contrast properties, with r_2/r_1 values in water much higher than those reported for most common SPION-based contrast agents. In addition, an excellent stability in time was demonstrated, the NMRD curves being perfectly reproducible for at least 2 months. Also considering the previously shown good biocompatibility of cetyl palmitate and the possibility of loading hydrophobic drugs in the same matrix,[38] the investigated systems seem of great potential for theranostic applications. On the basis of the present study, refinements of the preparation procedure should be proposed with the aim of better tuning the relaxometric properties of SPION-SLNs.

AUTHOR INFORMATION

Corresponding Author

*Address: Istituto di Chimica dei Composti OrganoMetallici, Sede Secondaria di Pisa, Consiglio Nazionale delle Ricerche − CNR, via G. Moruzzi 1, 56124 Pisa, Italy. E-mail: lucia.calucci@pi.iccom.cnr.it. Phone: +39 0503152517.

ORCID

Lucia Calucci: 0000-0002-3080-8807

Virgilio Mattoli: 0000-0002-4715-8353

Gianni Ciofani: 0000-0003-1192-3647

Author Contributions

The manuscript was written through contributions of all authors. All authors have given approval to the final version of the manuscript.

Notes

The authors declare no competing financial interest.

ACKNOWLEDGMENTS

Marco Carlo Mascherpa (ICCOM-CNR), Massimo Onor (ICCOM-CNR), and Massimo D'Orazio (Pisa University) are kindly acknowledged for performing ICP measurements. Alice Scarpellini (Istituto Italiano di Tecnologia) is gratefully acknowledged for technical assistance with TEM imaging. The authors thank Gattefossé (Italy) for providing cetyl palmitate. We are grateful to Beneficentia Stiftung for supporting the acquisition of the FFC relaxometer.

ABBREVIATIONS

SPION, superparamagnetic iron oxide nanoparticle; SLN, solid lipid nanoparticle; NMRD, nuclear magnetic relaxation dispersion; FFC, fast field-cycling

REFERENCES

(1) Mahmoudi, M.; Azadmanesh, K.; Shokrgozar, M. A.; Journeay, W. S.; Laurent, S. Effect of Nanoparticles on the Cell Life Cycle. *Chem. Rev.* **2011**, *111*, 3407−3432.

(2) Mahmoudi, M.; Hofmann, H.; Rothen-Rutishauser, B.; Petri-Fink, A. Assessing the In Vitro and In Vivo Toxicity of Superparamagnetic Iron Oxide Nanoparticles. *Chem. Rev.* **2012**, *112*, 2323−2338.

(3) Patil, U. S.; Adireddy, S.; Jaiswal, A.; Mandava, S.; Lee, B. R.; Chrisey, D. B. In Vitro/In Vivo Toxicity Evaluation and Quantification of Iron Oxide Nanoparticles. *Int. J. Mol. Sci.* **2015**, *16*, 24417−24450.

(4) Laurent, S.; Forge, D.; Port, M.; Roch, A.; Robic, C.; Vander Elst, L.; Muller, R. N. Magnetic Iron Oxide Nanoparticles: Synthesis, Stabilization, Vectorization, Physicochemical Characterizations, and Biological Applications. *Chem. Rev.* **2008**, *108*, 2064−2110.

(5) Mahmoudi, M.; Sant, S.; Wang, B.; Laurent, S.; Sen, T. Superparamagnetic Iron Oxide Nanoparticles (SPIONs): Development, Surface Modification and Applications in Chemotherapy. *Adv. Drug Delivery Rev.* **2011**, *63*, 24−46.

(6) Niemirowicz, K.; Markiewicz, K. H.; Wilczewska, A. Z.; Car, H. Magnetic Nanoparticles as New Diagnostic Tools in Medicine. *Adv. Med. Sci.* **2012**, *57*, 196−207.

(7) Thomas, R.; Park, I.-K.; Jeong, Y. Y. Magnetic Iron Oxide Nanoparticles for Multimodal Imaging and Therapy of Cancer. *Int. J. Mol. Sci.* **2013**, *14*, 15910−15930.

(8) Lam, T.; Pouliot, P.; Avti, P. K.; Lesage, F.; Kakkar, A. K. Superparamagnetic Iron Oxide Based Nanoprobes for Imaging and Theranostics. *Adv. Colloid Interface Sci.* **2013**, *199−200*, 95−113.

(9) Revia, R. A.; Zhang, M. Magnetite Nanoparticles for Cancer Diagnosis, Treatment, and Treatment Monitoring: Recent Advances. *Mater. Today* **2016**, *19*, 157−168.

(10) Wu, W.; Wu, Z.; Yu, T.; Jiang, C.; Kim, W.-S. Recent Progress on Magnetic Iron Oxide Nanoparticles: Synthesis, Surface Functional Strategies and Biomedical Applications. *Sci. Technol. Adv. Mater.* **2015**, *16*, 023501.

(11) Lee, N.; Yoo, D.; Ling, D.; Cho, M. H.; Hyeon, T.; Cheon, J. Iron Oxide Based Nanoparticles for Multimodal Imaging and Magnetoresponsive Therapy. *Chem. Rev.* **2015**, *115*, 10637−10689.

(12) Arami, H.; Khandhar, A.; Liggitt, D.; Krishnan, K. M. In Vivo Delivery, Pharmacokinetics, Biodistribution and Toxicity of Iron Oxide Nanoparticles. *Chem. Soc. Rev.* **2015**, *44*, 8576−8607.

(13) Kandasamy, G.; Maity, D. Recent Advances in Superparamagnetic Iron Oxide Nanoparticles (SPIONs) for In Vitro and In Vivo Cancer Nanotheranostics. *Int. J. Pharm.* **2015**, *496*, 191−218.

(14) Hauser, A. K.; Wydra, R. J.; Stocke, N. A.; Anderson, K. W.; Hilt, J. Z. Magnetic Nanoparticles and Nanocomposites for Remote Controlled Therapies. *J. Controlled Release* **2015**, *219*, 76−94.

(15) Laurent, S.; Saei, A. A.; Behzadi, S.; Panahifar, A.; Mahmoudi, M. Superparamagnetic Iron Oxide Nanoparticles for Delivery of Therapeutic Agents: Opportunities and Challenges. *Expert Opin. Drug Delivery* **2014**, *11*, 1449−1470.

(16) Laurent, S.; Dutz, S.; Häfeli, U. O.; Mahmoudi, M. Magnetic Fluid Hyperthermia: Focus on Superparamagnetic Iron Oxide Nanoparticles. *Adv. Colloid Interface Sci.* **2011**, *166*, 8−23.

(17) Grüttner, C.; Müller, K.; Teller, J.; Westphal, F. Synthesis and Functionalisation of Magnetic Nanoparticles for Hyperthermia Applications. *Int. J. Hyperthermia* **2013**, *29*, 777−789.

DOI: 10.1021/acs.jpcc.6b09562
J. Phys. Chem. C 2017, 121, 823−829

(18) Rauch, J.; Kolch, W.; Laurent, S.; Mahmoudi, M. Big Signals from Small Particles: Regulation of Cell Signaling Pathways by Nanoparticles. *Chem. Rev.* **2013**, *113*, 3391−3406.
(19) Gossuin, Y.; Gillis, P.; Hocq, A.; Vuong, Q. L.; Roch, A. Magnetic Resonance Relaxation Properties of Superparamagnetic Particles. *Wiley Interdiscip. Rev.: Nanomed. Nanobiotechnol.* **2009**, *1*, 299−310.
(20) Muller, R. N.; Vander Elst, L.; Roch, A.; Peters, J. A.; Csajbok, E.; Gillis, P.; Gossuin, Y. Relaxation by Metal-Containing Nanosystems. *Adv. Inorg. Chem.* **2005**, *57*, 239−292.
(21) Casula, M. F.; Floris, P.; Innocenti, C.; Lascialfari, A.; Marinone, M.; Corti, M.; Sperling, R. A.; Parak, W. J.; Sangregorio, C. Magnetic Resonance Imaging Contrast Agents Based on Iron Oxide Superparamagnetic Ferrofluids. *Chem. Mater.* **2010**, *22*, 1739−1748.
(22) Lee, N.; Hyeon, T. Designed Synthesis of Uniformly Sized Iron Oxide Nanoparticles for Efficient Magnetic Resonance Imaging Contrast Agents. *Chem. Soc. Rev.* **2012**, *41*, 2575−2589.
(23) Sharifi, S.; Seyednejad, H.; Laurent, S.; Atyabi, F.; Saei, A. A.; Mahmoudi, M. Superparamagnetic Iron Oxide Nanoparticles for in Vivo Molecular and Cellular Imaging. *Contrast Media Mol. Imaging* **2015**, *10*, 329−355.
(24) Lartigue, L.; Innocenti, C.; Kalaivani, T.; Awwad, A.; del Mar Sanchez Duque, M.; Guari, Y.; Larionova, J.; Guérin, C.; Georges Montero, J.-L.; Barragan-Montero, V.; et al. Water-Dispersible Sugar-Coated Iron Oxide Nanoparticles. An Evaluation of their Relaxometric and Magnetic Hyperthermia Properties. *J. Am. Chem. Soc.* **2011**, *133*, 10459−10472.
(25) Tong, S.; Hou, S.; Zheng, Z.; Zhou, J.; Bao, G. Coating Optimization of Superparamagnetic Iron Oxide Nanoparticles for High T_2 Relaxivity. *Nano Lett.* **2010**, *10*, 4607−4613.
(26) Tombácz, E.; Turcu, R.; Socoliuc, V.; Vékás, L. Magnetic Iron Oxide Nanoparticles: Recent Trends in Design and Synthesis of Magnetoresponsive Nanosystems. *Biochem. Biophys. Res. Commun.* **2015**, *468*, 442−543.
(27) Kolhatkar, A. G.; Jamison, A. C.; Litvinov, D.; Willson, R. C.; Lee, T. R. Tuning the Magnetic Properties of Nanoparticles. *Int. J. Mol. Sci.* **2013**, *14*, 15977−16009.
(28) Kralj, S.; Makovec, D. The Chemically Directed Assembly of Nanoparticle Clusters from Superparamagnetic Iron-Oxide Nanoparticles. *RSC Adv.* **2014**, *4*, 13167−13171.
(29) Shin, T.-H.; Choi, Y.; Kim, S.; Cheon, J. Recent Advances in Magnetic Nanoparticle-Based Multi-Modal Imaging. *Chem. Soc. Rev.* **2015**, *44*, 4501−4516.
(30) Ling, D.; Lee, N.; Hyeon, T. Chemical Synthesis and Assembly of Uniformly Sized Iron Oxide Nanoparticles for Medical Applications. *Acc. Chem. Res.* **2015**, *48*, 1276−1285.
(31) Arosio, P.; Thévenot, J.; Orlando, T.; Orsini, F.; Corti, M.; Mariani, M.; Bordonali, L.; Innocenti, C.; Sangregorio, C.; Oliveira, H.; et al. Hybrid Iron Oxide-Copolymer Micelles and Vesicles as Contrast Agents for MRI: Impact of the Nanostructure on the Relaxometric Properties. *J. Mater. Chem. B* **2013**, *1*, 5317−5328.
(32) Stepanov, A.; Burilov, V.; Pinus, M.; Mustafina, A.; Rümmeli, M. H.; Mendez, R. G.; Amirov, R.; Lukashenko, S.; Zvereva, E.; Katsuba, S.; et al. Water Transverse Relaxation Rates in Aqueous Dispersions of Superparamagnetic Iron Oxide Nanoclusters with Diverse Hydrophilic Coating. *Colloids Surf., A* **2014**, *443*, 450−458.
(33) Hak, S.; Goa, P. E.; Stenmark, S.; Bjerkholt, F. F.; Haraldseth, O. Transverse Relaxivity of Iron Oxide Nanocrystals Clustered in Nanoemulsions: Experiment and Theory. *Magn. Reson. Med.* **2015**, *74*, 858−867.
(34) Ebert, S.; Bannwarth, M. B.; Musyanovych, A.; Landfester, K.; Münnemann, K. How Morphology Influences Relaxivity - Comparative Study of Superparamagnetic Iron Oxide-Polymer Hybrid Nanostructures. *Contrast Media Mol. Imaging* **2015**, *10*, 456−464.
(35) Pereira, C.; Pereira, A. M.; Rocha, M.; Freire, C.; Geraldes, C. F. G. C. Architectural Design of Superparamagnetic Fe_3O_4 Nanoparticles for Application as MRI Contrast Agents: Masterizing Size and Magnetism for Enhanced Relaxivity. *J. Mater. Chem. B* **2015**, *3*, 6261−6273.
(36) Hickey, R. J.; Haynes, A. S.; Kikkawa, J. M.; Park, S.-J. Controlling the Self-Assembly Structure of Magnetic Nanoparticles and Amphiphilic Block-Copolymers: From Micelles to Vesicles. *J. Am. Chem. Soc.* **2011**, *133*, 1517−1525.
(37) Colombo, M.; Carregal-Romero, S.; Casula, M. F.; Gutiérrez, L.; Morales, M. P.; Böhm, I. B.; Heverhagen, J. T.; Prosperi, D.; Parak, W. Biological Applications of Magnetic Nanoparticles. *Chem. Soc. Rev.* **2012**, *41*, 4306−4334.
(38) Grillone, A.; Redolfi Riva, E.; Mondini, A.; Forte, C.; Calucci, L.; Innocenti, C.; de Julian Fernandez, C.; Cappello, V.; Gemmi, M.; Moscato, S.; et al. Active Targeting of Sorafenib: Preparation, Characterization, and In Vivo testing of Drug-Loaded Magnetic Solid Lipid Nanoparticles. *Adv. Healthcare Mater.* **2015**, *4*, 1681−1690.
(39) Geraldes, C. F. G. C.; Laurent, S. Classification and Basic Properties of Contrast Agents for Magnetic Resonance Imaging. *Contrast Media Mol. Imaging* **2009**, *4*, 1−23.
(40) Kim, H.; Dae, H.-M.; Park, C.; Kim, E. O.; Kim, D.; Kim, I.-H.; Kim, Y.-H.; Choi, Y. A Highly Sensitive Magnetite Nanoparticle as a Simple and Rapid Stem Cell Labelling Agent for MRI Tracking. *J. Mater. Chem.* **2011**, *21*, 7742−7747.
(41) Taylor, A.; Herrmann, A.; Moss, D.; Sée, V.; Davies, K.; Williams, S. R.; Murray, P. Assessing the Efficacy of Nano- and Micro-Sized Magnetic Particles as Contrast Agents for MRI Cell Tracking. *PLoS One* **2014**, *9*, e100259.
(42) Rohrer, M.; Bauer, H.; Mintorovitch, J.; Requardt, M.; Weinmann, H. J. Comparison of Magnetic Properties of MRI Contrast Media Solutions at Different Magnetic Field Strengths. *Invest. Radiol.* **2005**, *40*, 715−724.
(43) Jung, C. W.; Jacobs, P. Physical and Chemical Properties of Superparamagnetic Iron Oxide MR Contrast Agents: Ferumoxides, Ferumoxtran, Ferumoxsil. *Magn. Reson. Imaging* **1995**, *13*, 661−674.
(44) Qin, J.; Laurent, S.; Jo, Y. S.; Roch, A.; Mikhaylova, M.; Bhujwalla, Z. M.; Muller, R. N.; Muhammed, M. A High-Performance Magnetic Resonance Imaging T_2 Contrast Agent. *Adv. Mater.* **2007**, *19*, 1874−1878.
(45) Roch, A.; Muller, R. N.; Gillis, P. Theory of Proton Relaxation Induced by Superparamagnetic Particles. *J. Chem. Phys.* **1999**, *110*, 5403−5411.
(46) Gillis, P.; Roch, A.; Brooks, R. A. Corrected Equations for Susceptibility-Induced T_2-Shortening. *J. Magn. Reson.* **1999**, *137*, 402−407.
(47) Lévy, M.; Gazeau, F.; Wilhelm, C.; Neveu, S.; Devaud, M.; Levitz, P. Revisiting MRI Contrast Properties of Nanoparticles: Beyond the Superparamagnetic Regime. *J. Phys. Chem. C* **2013**, *117*, 15369−15374.
(48) Kruk, D.; Korpała, A.; Mehdizadeh Taheri, S.; Kozłowski, A.; Föster, S.; Rössler, E. A. ^{1}H Relaxation Enhancement Induced by Nanoparticles in Solutions: Influence of Magnetic Properties and Diffusion. *J. Chem. Phys.* **2014**, *140*, 174504.
(49) Sanz, B.; Calatayud, M. P.; Cassinelli, N.; Ibarra, M. R.; Goya, G. F. Long-Term Stability and Reproducibility of Magnetic Colloids Are Key Issues for Steady Values of Specific Power Absorption over Time. *Eur. J. Inorg. Chem.* **2015**, *2015*, 4524−4531.
(50) Kallumadil, M.; Tada, M.; Nakagawa, T.; Abe, M.; Southern, P.; Pankhurst, Q. A. Suitability of Commercial Colloids for Magnetic Hyperthermia. *J. Magn. Magn. Mater.* **2009**, *321*, 1509−1513.
(51) Pflipsen, C.; Forge, D.; Benali, S.; Gossuin, Y. Improved Stability of Relaxivity of a Commercial Magnetic Ferrofluid. *J. Phys. Chem. C* **2013**, *117*, 20919−20926.
(52) Anoardo, E.; Galli, G.; Ferrante, G. Fast-Field-Cycling NMR: Applications and Instrumentation. *Appl. Magn. Reson.* **2001**, *20*, 365−404.
(53) Kimmich, R.; Anoardo, E. Field-Cycling NMR Relaxometry. *Prog. Nucl. Magn. Reson. Spectrosc.* **2004**, *44*, 257−320.
(54) Roch, A.; Moiny, F.; Muller, R. N.; Gillis, P. Water Magnetic Relaxation in Superparamagnetic Colloid Suspensions: the Effect of Agglomeration. *NATO Sci. Ser., II* **2002**, *76*, 383−392.
(55) Holz, M.; Heil, S. R.; Sacco, A. Temperature-Dependent Self-Diffusion Coefficients of Water and Six Selected Molecular Liquids for

DOI: 10.1021/acs.jpcc.6b09562
J. Phys. Chem. C 2017, 121, 823−829

Calibration in Accurate ^{1}H NMR PFG Measurements. *Phys. Chem. Chem. Phys.* **2000**, *2*, 4740−4742.
(56) Roch, A.; Gossuin, Y.; Muller, R. N.; Gillis, P. Superparamagnetic Colloid Suspensions: Water Magnetic Relaxation and Clustering. *J. Magn. Magn. Mater.* **2005**, *293*, 532−539.
(57) Vuong, Q. L.; Berret, J.-F.; Fresnais, J.; Gossuin, Y.; Sandre, O. A Universal Scaling Law to Predict the Efficiency of Magnetic Nanoparticles as MRI T2-Contrast Agents. *Adv. Healthcare Mater.* **2012**, *1*, 502−512.

DOI: 10.1021/acs.jpcc.6b09562
J. Phys. Chem. C 2017, 121, 823−829